On the use of exploratory models to survey complicated problems: from atomic collisions to the properties of dense molecular hydrogen

Salvador A. Cruz

Programa de Simulación Molecular, Instituto Mexicano del Petróleo
Apartado postal 14-805, 07730 México, D.F., Mexico
Departamento de Física, Universidad Autónoma Metropolitana-Iztapalapa
Apartado postal 55-534, 09340 México, D.F., Mexico
e-mail: scruz@www.imp.mx; cruz@xanum.uam.mx

Most of the problems in contemporary physics research become complicated due to their many-body character and require of an involved treatment which—in many cases—leads to equally complicated algorithms encripting the physics before a partial solution is obtained. The purpose of this paper is to remind on the usefulness of simple exploratory models for the analysis of complex problems before a more sophisticated approach is developed. In this spirit, three examples are reviewed from the perspective of the author's experience: (*i*) molecular effects in the stopping power of heavy ions, (*ii*) quantum-size effects in Wannier excitons and (*iii*) pressure effects on the properties of molecular hydrogen. In the latter case, new results are reported for the electronic and vibrational properties of the ground-state hydrogen molecule in a padded spherical box on the basis of a simple molecular confinement model.

Keywords: Stopping power; atomic collisions; excitons; quantum dots; molecular cinfinement; high pressures

La mayoría de los problemas contemporáneos de investigación en física son complejos debido a las interacciones de muchos cuerpos, requiriendo en general de tratamientos sofisticados, los cuales en muchas ocasiones conducen al desarrollo de algoritmos igualmente complicados en los que queda encriptada la física antes de obtener una solución parcial. El propósito de este trabajo es el de recordar sobre la utilidad del uso de modelos exploratorios simples para el análisis de problemas complicados, previo al desarrollo de tratamientos más elaborados. Dentro de este espíritu, se revisan tres ejemplos que de acuerdo a la experiencia del autor pueden ser de interés: (*i*) efectos moleculares en el poder de frenamiento de iones pesados, (*ii*) efectos cuánticos de restricción espacial en excitones de Wannier y (*iii*) efecto de presión sobre las propiedades del hidrógeno molecular. En el último caso, empleando un modelo de confinamiento molecular sencillo, se reportan resultados novedosos para las propiedades electrónicas y vibracionales del estado base de la molécula de hidrógeno confinada por una pared esférica penetrable.

Descriptores: Poder de frenamiento; colisiones atómicas; excitones; puntos cuánticos; confinamiento molecular; altas presiones

1. Introduction

The advent of new—more powerful and sophisticated—computational resources, as well as experimental techniques, has motivated a deeper quest into complex problems whose many-body character requires of special treatment. This is the case in a great variety of problems in condensed matter physics, where the atomic and molecular structure play an impotant role to establish the properties of a medium and the way it responds to external perturbations. In this connection, the techniques of quantum chemistry have proven to be very useful in dealing satisfactorily with extended systems formed by a great number of atoms and where many-body interactions are incorporated by solving selfconsistently the corresponding Schröedinger equation. Without digressing too much, let me mention that there are, of course, other *ab-initio* methods developed to analyze collective interactions and the properties of condensed matter systems, such as the quantum Monte Carlo method (QMC) [1] and *ab-initio* molecular dynamics (AIMD) [2], among others. In all cases, the actual limitation for the size of the system under study is dictated mainly by the computational resources.

Although the most realistic treatment of a problem certainly requires of an approach with increasing complexity, quite frequently the physics inherent to the problem remains encripted in an algorithm or a numerical output demanding for interpretation. This is critical when a new idea is put forward, since a first survey of its adequacy should be advanced before embarquing in a detailed calculation. To this end, it is worth resorting to exploratory models whereby the relevant physical quantities are clearly defined. An exploratory model—if physically plausible—allows for proper orientation on the relative importance of the various relevant physical quantities involved. It also helps keeping the physical perspective of the problem and its potentiality. Surprisingly, a successful exploratory model may work better than expected both, qualitatively and quantitatively, when compared to more sophisticated treatments.

The purpose of this contribution is to remind on the usefulness of simple exploratory models for the treatment of complicated problems before more powerful treatments are deployed. To this end, the author reviews three different research problems where he has experienced the value of exploratory models. The first problem is presented in Sect. 2,

and deals with chemical bond effects on the energy loss of heavy ions while penetrating compound target materials. In Sect. 3, semiconductor microcrystal quantum-size effects on the energy levels of Wannier excitons are treated. In Sect. 4, the pressure effects on the properties of molecular hydrogen are discussed on the basis of a molecular confinement model. Finally, the concusions of this paper are presented in Sect. 5.

Due to the different characteristics of the problems reviewed in this paper, major emphasis is kept in presenting the main reasoning leading to the development of the corresponding exploratory model and its predictions. A detailed discussion is achievable through the source references. In spite of this, complementary new results for the polarizability and vibrational properties of compressed molecular hydrogen obtained with the model discussed in Sect. 4 are reported.

2. Chemical bond effects on the low-energy electron stopping power of heavy ions

When a zwift ion penetrates matter, it loses energy through interactions with atoms and molecules forming the medium. These interactions involve, of course, electrons and nuclei. Assuming no nuclear reactions take place, the projectile-target electron interactions play a dominant role in the stopping process (dE/dx) (inelastic or electronic stopping). This happens for a wide range of projectile energy values going from high to low energies, whereas the elastic (or nuclear) stopping becomes dominant only at very low energies and is due to changes in trajectory imposed by the interatomic potentials of the already neutralized projectile-target system. Figure 1 shows schematically a typical electronic stopping curve where the electronic stopping cross section for a medium with n-scatterers per unit volume is defined as [3]:

$$S_e = -\frac{1}{n}\frac{dE}{dx} \qquad (1)$$

From Fig. 1, three characteristic regions are observed in the stopping curve. The high-energy regime (Region III), where the projectile practically remains as a bare charged particle and loses energy through ionization processes induced in the target. The intermediate energy regime (Region II), where electron-capture and loss, inner shell excitation, electron promotion and ionization mechanisms are admixtured and the low-energy regime (Region I), in which projectile and target are practically neutral and the stopping process is more like that of a viscous interface. Clearly, the many-body character of the problem demands of judicious approximate treatments. It was Hans Bethe, in 1930 [4], who made the first successful approximate quantum mechanical approach to the high-energy energy loss problem, demonstrating that the main source of energy loss in this region comes from individual target-atom ionization. Since then, the theory has been substantially advanced by different groups in the world, although still no satisfactory theory exists to account for the whole energy dependence of the various processes [3, 5].
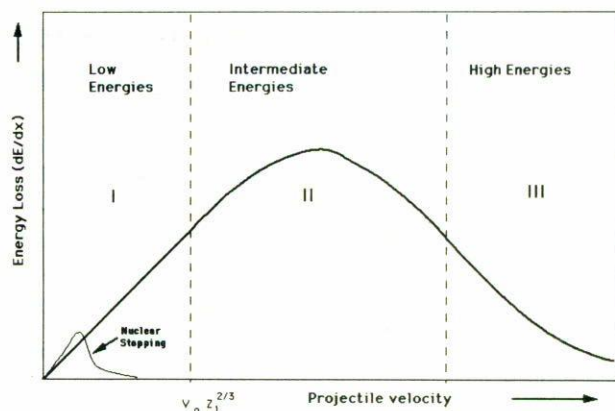
FIGURA 1. Typical stopping power curve for ions traversing a given material. Three different regions are identified according to the ion energy where different stopping processes participate (see text). Note the region of dominance for nuclear stopping. The low-energy region is currently defined for ion velocities $v \leq v_0 Z_1^{2/3}$ where Z_1 is the ion atomic number and v_0 the Bohr velocity.

An additional problem, noticed relatively recently after the advent of more precise experimental measurement techniques, is the non-additivity of atomic contributions to the electronic stopping cross section in the case of compound materials [6]. Furthermore, target physical phase state effects in Se play also an important role. These two effects are relevant for projectile energies in the region below and around the maximum of the stopping curve [7–9]. New ideas on the partitioning of the stopping contribution into cores and bonds (CAB) were put forward by various authors [10–15]. The first fundamental theoretical study to account for the degree of participation of different bond types on proton stopping in hydrocarbons was achieved by Oddershede and Sabin in 1987 [12, 13]. The first theoretical treatment of molecular effects on heavy ion stopping in the low-energy region was done in 1993 by the present author and his collaborators [16] using a relatively simple model which allows for a qualitative and quantitative insight on the role of chemical bonds and projectile structure on the stopping process. As the reader must be aware, the task in performing a detailed calculation for such a many-body problem is formidable and perhaps could only be accomplished by a dynamical quantum chemistry calculation [17, 18]. The main assumptions of the model as well as some of the relevant results are discussed below. Further details may be found in Ref. 16.

2.1. The Firsov model

Suppose a given projectile, which has become practically neutralized after a series of collision events and is moving with an energy low enough such that in each individual encounter with a target atom or molecule, a deceleration takes place due to a drag force produced by momentum exchange involving projectile and target electrons. Owing to the indistinguishability of electrons, this momentum exchange could be regarded as an electron exchange, i.e. as projectile and
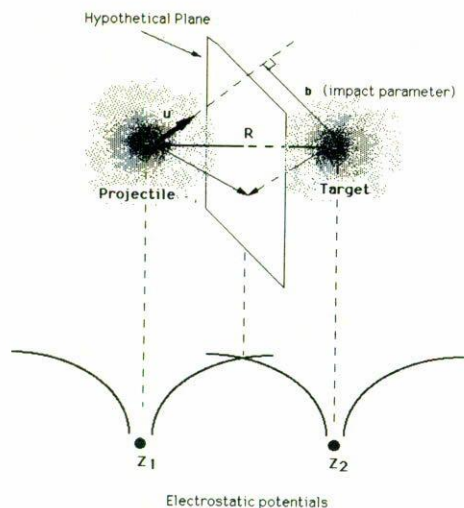
FIGURE 2. Schematic diagram showing the location of the hypothetical Firsov plane between projectile and target at the point where the electrostatic potentials are equal.

target approach each other, their electronic clouds start overlapping and an electron which originally belonged to one of the systems, suddenly switches its parent atom carrying with it a momentum $m\mathbf{u}$, where m is the electron mass and $\mathbf{u}$ the relative velocity of the two systems. The drag force is obtained in terms of the flux of momentum ψ due to both projectile and target electrons. This idea was first proposed by O.B. Firsov in 1959 [19] for low-energy stopping. Viewing projectile and target as two Thomas-Fermi atoms, Firsov calculated the momentum flux from one system to another by locating a hypothetical plane perpendicular to the line joining the nuclei and at a position where both the projectile and target electrostatic potentials coincide (see Fig. 2). The inelastic energy transfer $\varepsilon(b)$ in a collision, for a given impact parameter b, corresponds to the work of slowing down:

$$\varepsilon(b) = m \int \mathbf{u} \cdot d\mathbf{R} \int d\phi, \qquad (2)$$

where $\mathbf{R}$ is the relative position vector between target and projectile and the flux integration is performed over the hypothetical plane taking into account both the projectile and target electron velocity distributions [20]. The electronic stopping cross section S_e is then obtained as:

$$S_e = 2\pi \int \varepsilon(b) b \, db. \qquad (3)$$

An interesting feature of this model is the possible distinction between the flux contribution from projectile and target, *i.e.* the total electronic stopping cross section may be written as:

$$S_e = S_{e,p} + S_{e,t} \qquad (4)$$

where the indices p and t stand for projectile and target, respectively.

The adequacy of this simple model to describe experimental measurements in the low-energy stopping regime has

been widely accepted. In this connection, let me briefly mention that another important model based on the dielectric response formalism was successfully developed by J. Lindhard in 1954 [21, 22] whereby the induced electric field in the material produces a retarding force on the projectile. The interested reader is kindly addressed to Ref. 3 for a review. We now return to our main point of discussion.

Firsov's idea is adequate for the treatment of molecular stopping since it distinguishes between projectile and target properties. In fact, in 1979 D.K. Brice and the present author generalized Eqs. (2) and (3) to account for molecular stopping using a proper quantum description for the probability current of bound-state wavefunctions in one direction across the hypothetical surface and considering angular averaging over all molecular orientations [23]. The model was applied only to molecular hydrogen using a LCAO representation of the molecular wavefunction. However, this molecular representation made the mathematical treatment too involved and only a non trivial numerical solution could render the final values for the molecular contribution to S_e for H_2. The answer for other systems had to wait almost fifteen years until a reasonable model for the molecular representation was used as described below.

2.2. The FSGO representation of localized molecular orbitals

The floating spherical Gaussian orbital (FSGO) model was first introduced by A. Frost in 1967 [24] in the *ab-initio* study of the electronic and geometric structure of ground state closed-shell molecules using localized orbitals. Within this scheme, each doubly occupied localized orbital Φ_k is represented by a single normalized spherical Gaussian:

$$\Phi_k(\mathbf{r} - \mathbf{R}_k) = \left(\frac{2}{\pi\sigma_k^2}\right)^{3/4} \exp\left[\frac{-(\mathbf{r} - \mathbf{R}_k)^2}{\sigma_k^2}\right], \qquad (5)$$

where σ_k is the radius of the orbital and $\mathbf{R}_k$ the position of its center. The set of orbitals $\{\Phi_i\}$ is non-orthogonal and, according to Frost, if $\mathbf{S}$ is the overlap matrix of the set and $\mathbf{T} = \mathbf{S}^{-1}$ its inverse, then the electronic energy for the molecule is [25]:

$$E_{\text{el}} = 2\sum_{j,k}(j|k)T_{jk} + \sum_{k,\ell,p,q}(k\ell|pq)[2T_{k\ell}T_{pq} - T_{kq}T_{\ell p}] \qquad (6)$$

where $(j|k)$ are the one-electron integrals and $(kl|pq)$ the two-electron coulomb and exchange terms given as

$$(kl|pq) = \int \Phi_j w \Phi_k \, dv \qquad (7a)$$

$$(kl|pq) = \int \Phi_k(1)\Phi_\ell(1)r_{12}^{-1}\Phi_p(2)\Phi_q(2) \, dv_1 \, dv_2 \qquad (7b)$$

with w the one-electron operator accounting for kinetic energy and electron-nuclear attraction, *i.e.* (atomic units):

$$w = -\frac{1}{2}\nabla^2 - \sum_\nu \frac{Z_\nu}{r_\nu}, \qquad (7c)$$
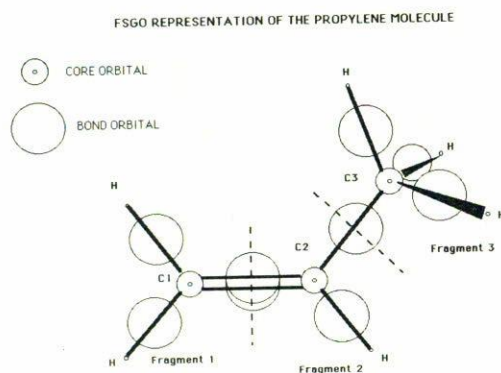
FIGURE 3. Doubly occupied Core and bond localized molecular orbitals in the floating spherical Gaussian orbital (FSGO) representation of the propylene molecule. Three functional groups are identified as molecular fragments (see text).

FIGURE 4. Schematic representation of the use of molecular fragments to locate the corresponding hypothetical Firsov plane relative to the projectile in the calculation of molecular stopping.

Z_ν being the charge of nucleus ν and r_ν the corresponding electron-nucleus distance. After adding the internuclear repulsion energy, the total energy becomes

$$w = E_{\rm el} + \sum_{\lambda < \nu} \frac{Z_\lambda Z_\nu}{r_{\lambda\nu}}, \qquad (8)$$

In general, the total energy will be a function of the orbital radius (σ_k), orbital positions ($\mathbf{R}_k$) and nuclear positions ($\mathbf{r}_\nu$). Energy minimization relative to all quantities ($\sigma_k, \mathbf{R}_k, \mathbf{r}_\nu$) provides the parameters defining the corresponding molecular configuration. According to Frost, the use of a single gaussian orbital per electron pair constitutes a subminimal basis and hence the molecular energies are typically about 20% above the Hartree-Fock value. In spite of this, the electron density and molecular geometry are reasonably well described. Using this procedure, Frost and coworkers reported molecular parameters for a wide number of systems [24]. Figure 3 shows schematically the FSGO representation of core and bond orbitals for the propylene molecule. Clearly, the simple analytical expression for each orbital and the individual orbital assignement to each molecular moiety (cores, bonds and lone-pairs) are very useful characteristics of the FSGO representation. Note also from Fig. 3 that some functional groups may be distinguished and labeled as "fragments" (see below).

2.3. The model for molecular stopping

In constructing our exploratory model for molecular stopping, two major issues had to be solved:

i) a proper description of atomic and molecular orbitals which should be simple and tractable

ii) a reasonable criterion to define the hypothetical surface for flux evaluation.

Regarding point (*i*), for the molecular target the FSGO representation of localized molecular orbitals was chosen. For the atomic projectile orbitals, the analytical Hartree-Fock-Slater representation [26] was used.
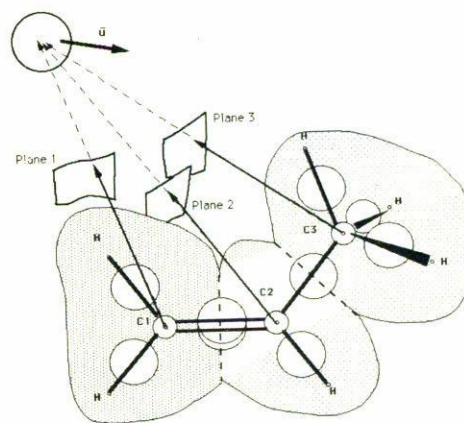
Concerning the position of the hypothetical surface [point (*ii*) above], the concept of molecular fragments was used [14, 16]. A molecular fragment corresponds to a molecular entity describable through localized orbitals acting as a functional group within the molecule. Within the FSGO approach, a molecular fragment corresponds to the region centered on the nucleus of a heavy atom where the core and other orbitals pack together (see Fig. 3). For each molecular fragment-projectile combination a given hypothetical surface was set at a position dictated by the matching of the corresponding electrostatic potentials [16]. Figure 4 shows schematically this situation for an atomic projectile colliding with a propylene molecule. The molecular fragments in this figure are enclosed by shadowed areas for visual clarity.

The momentum flux evaluation for both projectile and target was carried out through the previously generalized expression of Eqs. (2) and (3) [14, 23]. I would like to stress at this stage that, although these last steps required of previous laborious work, the final clue to achieve a surveying answer was the procedure mentioned further above.

Tables I–III display the predictions of the model described here for He and Li projectiles incident on several hydrocarbons and simpler molecular targets with a velocity $\nu = \nu_0$ (ν_0 is the Bohr velocity) [14–16]. Also shown in this table are corresponding available experimental data. The general agreement with experiment is reasonable, in spite of the simplicity of the exploratory model employed. Note that no adjustable parameters are used throughout the calculation. An important outcome of this simplified treatment is the possibility to analyze the relative importance of core, bond and lone-pair orbitals in the stopping process. Table IV displays, as an example, these quantities for NH_3, H_2O, CO, N_2 and H_2S and a set of low-energy heavy projectiles. In all these cases the molecule was considered as a single fragment. For second-row atoms the K and L shells need a special treatment within the FSGO approach so that sp^3 hybridization is taken into account [27]. In this case, the K and L-shell contributions ($S_{K \, {\rm shell}}$, $S_{L \, {\rm shell}}$) to stopping must be calculated in

TABLE I. Comparison between experiment and theory for the electronic stopping cross section for He and Li incident on various hydrocarbons at $v = v_0$. All units in 10^{-15} eVcm^2/molecule. (Reproduced from Ref. 16.

Molecule	Formula	Helium		Lithium	
		This work	Exp.[a]	This work	Exp.[a]
Alkanes					
Methane	CH_4	42.3	50.9	67.2	—
			50.0		
			46.3		
Ethane	C_2H_6	76.9	85.0	124.6	124.8
			76.6		
Propane	C_3H_8	111.5	121.9	182.0	163.7
			122.4		
n-butane	C_4H_{10}	146.1	158.1	239.4	209.0
n-pentane	C_5H_{12}	180.7	—	296.7	263.6
n-hexane	C_6H_{14}	215.3	—	354.1	313.3
n-heptane	C_7H_{16}	249.9	—	411.4	356.2
n-octane	C_8H_{18}	284.5	—	468.8	408.0
n-pentadecane	$C_{15}H_{32}$	526.7	—	870.4	740.0
isooctane	C_8H_{18}	253.8	—	416.4	407.0
Cyclopropane	C_3H_6	103.8	103.9	172.1	144.9
			111.5		
			102.3		
Cyclobutane	C_4H_8	138.4	—	229.5	—
Cyclopentane	C_5H_{10}	173.0	177.3	286.8	244.5
Cyclohexane	C_6H_{12}	207.6	213.0	344.2	291.3
Cycloheptane	C_7H_{14}	242.1	—	401.6	336.4
Cyclooctane	C_8H_{16}	276.7	285.8	458.9	386.7
Alkenes					
Ethylene	C_2H_4	69.3	72.2	115.4	102.4
			73.9		
			65.3		
Propylene	C_3H_6	103.9	108.7	172.7	150.0
			109.8		
Butene	C_4H_8	138.5	—	230.0	—
Pentene	C_5H_{10}	173.1	—	287.4	246.9
Hexene	C_6H_{12}	207.7	—	344.8	295.5
Cyclopropene	C_3H_4	96.1	—	162.7	—
Cyclobutente	C_4H_6	130.7	—	220.1	—
Cyclopentene	C_5H_8	165.3	163.4	277.4	227.5
Cyclohexene	C_6H_{10}	192.2	202.6	325.4	272.9
Allene	C_3H_4	96.2	102.1	163.3	—
1●3-Butadiene	C_4H_6	130.8	133.4	220.7	—
1●3-Cyclo hexadiene	C_6H_8	200.0	188.8	334.8	—
Alkynes					
Acetylene	C_2H_2	60.8	63.0	104.4	—
			63.7		
			57.3		
Aromates					
Benzene	C_6H_6	184.5	181.3	316.1	239.1
Toluene	C_7H_8	219.0	215.9	373.2	285.4
Phenylacetylene	C_8H_6	237.4	229.8	410.2	—

[a] See Ref. 16 for details.

TABLE II. Comparison between theory and experiment for the total electronic stopping cross section of He ions incident on alcohol and amine molecules at $v = v_0$, All units are in 10^{-15} eVcm^2/molecule. (Reproduced from Ref. 15).

Molecule	Formula	Theory	Experiment[a]
Alcohols			
Methanol	CH_3OH	62.9	71.8
Ethanol	C_2H_5OH	97.5	107.3
Propanol	C_3H_7OH	132.0	143.2
Dimethylether	C_2H_6O	97.1	107.8
Diethylether	$C_4H_{10}O$	166.7	177.7
Amines			
Methylamine	CH_3NH_2	67.1	80.7
Dimethylamine	$(CH_3)_2NH$	101.3	119.5
Trimethylamine	$(CH_3)_3N$	135.5	147.4
Ethylamine	$CH_3CH_2NH_2$	101.7	117.9

[a] See Ref. 15 for details.

TABLE III. Comparison between theory and experiment for the total electronic stopping cross section of He and Li projectiles incident on some simple molecular targets $(v = v_0)$. All units in 10^{-15} eVcm^2/molecule. (Reproduced from Ref. 16).

Projectile	Molecule	Theory	Experiment[a]
He	N_2	50.2	49.7
			45.0
			40.6
He	O_2	47.7	47.3
			44.8
			38.7
He	CO	43.7	48.8
			43.9
He	H_2O	32.1	36.5
Li	H_2O	58.0	46.8
He	NH_3	33.0	44.3
He	H_2S	48.5	62.1

[a] See Ref. 16 for details.

place of that for core electrons [16]. Figure 5 shows the predicted stopping cross section behavior for different projectiles (Z_p) impinging on gaseous ethane (C_2H_6) and toluene (C_7H_8) targets with $\nu = \nu_0$. Also included in this figure are corresponding predictions by the TRIM90 computer code generated by Ziegler *et al.* [11] who used a semiempirical scaling approach for the partitioning of core and bond contributions to S_e. For light projectiles ($Z_p \leq 5$) reasonable agreement between both calculations is observed. However, strong quantitative and qualitative differences are observed for heavier projectiles. Unfortunately, so far no experiments have been carried out for heavier ions than He and Li in order to assess definite conclusions on this discrepancy.

In concluding this section, it is worth to be aware of the limitations of the approximations made to survey such complicated problem. First, we have assumed that both, projectile

TABLE IV. Core, bond and lone-pair contributions to the stopping cross section for some low-energy ($v = v_0$) heavy projectiles in simple molecular targets. All units in 10^{-15} eVcm^2/bond. (Reproduced from Ref. 16).

Z_p	O–H (H$_2$O)	N–H (NH$_3$)	C≡O (CO)	N≡N (N$_2$)	O=O (O$_2$)	S–H (H$_2$S)	L_p(O)	L_p(N)	L_p(C)	L_p(S)	O	N	C	$S_{K\,shell}$	$S_{L\,shell}$
2	3.945	5.231	11.876	17.739	9.976	6.588	3.818[a] 3.878[b] 3.521[c]	4.754[d] 4.748[e]	4.888	6.086	0.377	0.471	0.607	0.147	2.428
3	6.379	9.379	19.329	20.805	15.963	12.041	6.707[a] 6.326[b] 5.641[c]	6.336[d] 5.335[e]	6.023	11.607	0.430	0.556	0.735	0.162	2.701
7	8.262	9.025	26.993	30.786	22.381	16.347	9.237[a] 8.411[b] 7.535[c]	9.019[d] 7.531[e]	8.239	9.773	0.622	0.879	1.183	0.210	3.585
8	8.181	11.920	26.699	30.310	22.182	15.876	9.010[a] 8.345[b] 7.488[c]	8.833[d] 7.454[e]	8.153	9.580	0.646	0.914	1.201	0.219	3.736

[a] H$_2$O   [b] CO   [c] O$_2$ [d] NH$_3$ [e] N$_2$
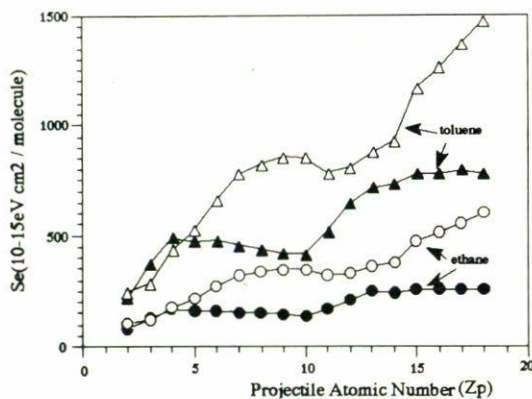
FIGURE 5. Electronic stopping cross section versus projectile atomic number (Z_p) for ethane (C$_2$H$_6$) and toluene (C$_7$H$_8$) as predicted by the exploratory model described in this work (full circles and triangles). Open circles and triangles are the predictions by Ziegler *et al.* [11]. (Replotted from Ref. 16).

and target retain all their electrons during the collision process (only momentum transfer is considered). Hence no charge capture and loss mechanisms are taken into account. Also, no electron promotion mechanisms in projectile and target are incorporated. In spite of this, we have been able to explore some of the characteristics of heavy ion stopping in compound materials at low energies.

3. Confinement of excitons in spherical quantum dots

The actual techniques for preparation of nanostructured materials have opened an exciting spectrum of new properties due to the reduced dimensions of the physical systems involved (several atomic diameters), where quantum effects dominate. On the other hand, these systems of reduced di-

mension are mostly embedded in a medium which in turn has a given atomic or molecular structure. Hence, a detailed study of the properties of nanostructures involves once again many-body interactions. In this section, a simplified exploratory model to survey quantum size effects on the ground-state energy of excitons trapped within semiconductor microcrystallites of spherical shape is presented. Further details may be assessed from Ref 28.

A great deal of theoretical and experimental work has been devoted to study the changes in optical properties of semiconductor microcrystallites as compared to those of the bulk material. It is deemed that electronic excitations in an inorganic semiconductor take place through loosely bounded electron-hole pairs called Wannier-Mott (WM) excitons. A characteristic of WM excitons is their strong delocalized nature over the crystal, the *e-h* correlation distance (D_B) being much larger than the crystal lattice constant. Hence, as the crystal size is reduced and approaches D_B, quantum size effects on the *e-h* pair start becoming dominant. The various theoretical approaches employed to analyze the size dependence of the energy levels of excitons confined by spherical quantum dots differ in degree of sophistication and it would be impossible to give a complete account here. Let me simply state here that, for the purposes of this paper, it suffices to discuss a very simple exploratory model proposed by Marin, Riera and this author, based on the use of the direct variational method. For information on other equally important treatments, the reader is kindly addressed to Refs. 29–37.

3.1. The model

Consider a WM exciton confined within a microcrystallite of spherical shape, of radius r_0 embedded in an insulating material. Assuming the validity of the effective mass approximation (EMA) in the single-band scheme for all values of

r_0, a spherical shape and the same dielectric constant ε for the crystallite as that of the bulk material, the model Hamiltonian for the system is written as (we shall consider here $\hbar = e = 1$) [28]:

$$\hat{H} = -\frac{1}{2m_3}\nabla_e^2 - \frac{1}{2m_h}\nabla_h^2 - \frac{1}{\varepsilon|r_e - r_h|} + V_e + V_h, \quad (9)$$

where m_e and m_h are the electron and hole effective masses relative to the free-electron mass, r_e and r_h their respective positions from the centre of the sphere and V_e, V_h are the barrier heights associated to the confining potential for electron and hole, respectively. Neglecting surface and image potential effects, we can consider the same barrier height for electron and hole, *i.e.* the confining potential for this system is treated as:

$$V_e = V_h = \begin{cases} 0 & r_e, r_h \leq r_0 \\ V_0 & r_e, r_h > r_0 \end{cases} \quad (10)$$

This confining potential step may be interpreted as an average effect due to a difference in composition between the crystallite and the host material.

The simplest approach to survey the quantum-size effects on the exciton energy is to use the direct variational method with a proper ansatz wavefunction subject to the corresponding boundary conditions. The variational method has been widely used to tackle this problem, mainly using Hylleraas coordinate transformations [32, 33, 35] or single-particle wavefunction expansions [36, 37]. A much simpler exploratory approach consists in recognizing that the structure of the Hamiltonian given by Eq. (9) is analogous to that for the helium atom, except for the attractive e-h interaction and zero nuclear charge in this case. This suggests that the ground state wavefunction for the helium atom may be used as a first trial wavefunction. Accordingly, the ground-state wavefunction for the e-h system in the interior region was proposed in [28] as:

$$\Psi_i = A \exp[-\alpha(r_e + r_h)](r_0 - \alpha r_e)(r_0 - \alpha r_h);$$
$$(r_e, r_h \leq r_o) \quad (11a)$$

and for the exterior region:

$$\Psi_o = B(r_e r_h)^{-1}\exp[-\beta(r_e + r_h)]; \quad (r_e, r_h > r_o) \quad (11b)$$

where A and B are normalizing factors and α and β are variational parameters. The multiplying factors to the right of the exponential term in Eq. (11a) are introduced to warrant that the wavefunction goes to zero at the boundary when the potential barrier height becomes infinite [38, 39].

The following subsidiary continuity condition on the wavefunction and consevation of probability current across the boundary is imposed:

$$\frac{1}{m_i}\frac{1}{\psi_i}\frac{\partial \psi_i}{\partial r_s} = \frac{1}{m_o}\frac{1}{\psi_o}\frac{\partial \psi_i}{\partial r_s} \quad \text{at} \quad r_s = r_o; s = e, h \quad (12)$$

where $m_i(m_o)$ correspond to the interior (exterior) reduced effective mass of the exciton to account for different electron
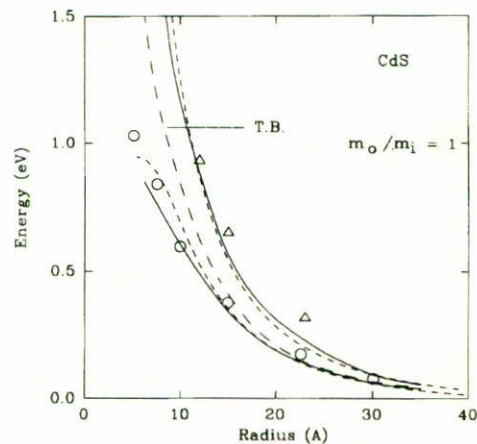
FIGURE 6. Exciton energy in CdS crystallites as a function of their size. Symbols represent experimental measurements performed in different host materials: (O) organic [30], ($\triangle$) silicate glass [42]. (—) EBOM calculations [31] ($V_0 = 2.25\,eV$ for higher curve; $V_0 = 0.5$ eV for lower curve). (- - -) Model described here [28] ($V_0 = 2.25$ eV for higher curve; $V_0 = 0.475$ eV for lower curve). (Replotted from Ref. 28).

and hole effective masses in two regions with different composition [36]. In fact, the variational parameters α and β are related through Eq. (12) as:

$$\beta = \frac{\left(\dfrac{m_o}{m_i}\right)[\alpha(1 - \alpha)r_0 + \alpha] + \alpha - 1}{(1 - \alpha)r_o} \quad (13)$$

hence it is only required to minimize the energy with respect to one variational parameter.

3.2. Three cases: CdS, CdSe, and PbS crystallites

The energy functional expression may be obtained analytically and the numerical values for the variational parameters are obtained through a simple numerical search routine. Figures (6)–(8) show the predictions of this model for the exciton ground-state energy for various crystallites embedded in different host materials as a function of their size. Also shown are corresponding experimental data as well as other theoretical predictions based on more detailed calculations. While the experimental data and relevant quantities are properly indicated in the figures, a brief description of the various theoretical approaches is worth mentioning. For the CdS crystallites (Fig. 6), the theoretical calculations by Einevoll [31] (continuous line) are based on a finite-barrier-height potential and the effective bond-orbital method (EBOM) for the hole and the effective-mass approximation (EMA) for the electron. On the other hand, the corresponding calculations by Lippens and Lanoo [34] (labeled T.B.) make use of the tight-binding method using an infinite-barrier-height potential. The predictions of our exploratory model (assuming $m_o/m_i = 1$) are given by the dashed curves. In the case of CdSe crystallites (Fig. 7), the theoretical predictions by Wang
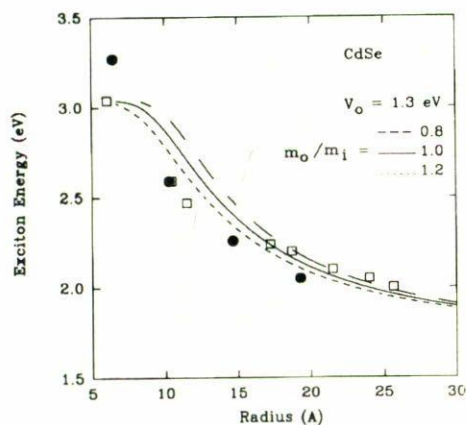
FIGURE 7. Exciton energy in CdSe crystallites as a function of their size. ($\square$) Experimental data [40]. ($\bullet$) pseudopotential calculations [40]. Curves correspond to the predictions of the model described here [28] for different ratios m_o/m_i (see text). (Replotted from Ref. 28).
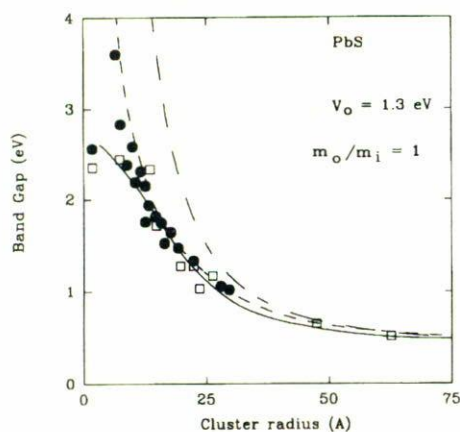
FIGURE 8. Band gap (exciton energy) for a PbS cluster as a function of its size. Uppermost curve: empirical EMA calculation from Ref. 29. ($\square$) Experimental data [41]. ($\bullet$) Cluster tight binding calculations [41]. (- - -) Hyperbolic band calculation [41]. (—) Results of the work described here [28]. (Replotted from Ref. 28).

and Zunger [40] (solid circles) are done through a plane-wave semiempirical pseudopotential method (SEPM) with non-local potentials and spin-coupling and assuming a size-dependent dielectric constant in the Coulomb interaction energy. In this figure, while keeping a reasonable trend with experiment, our predictions for different values for m_o/m_i show a sensitivity to differences in the interior and exterior exciton reduced effective mass induced by compositional differences with the host material. Finally, for PbS crystallites (Fig. 8) an empirical EMA calculation (uppermost curve), a cluster tight-binding calculation (solid circles) and a hyperbolic band calculation (dashed line) by Wang and Herron [29] and Wang et al. [41] are shown. The solid curve represents the results obtained with the model presented here.

Interestingly enough from the above mentioned figures, the qualitative and quantitative agreement observed with ex-

periment as well as with other, more sophisticated theoretical treatments, is very rewarding. In spite of the simplicity of the model, the general features of quantum-size effects on excitonic behavior are conserved. Again, no adjustable parameters have been used, only for the experimental band-gap width whis is used as a baseline to compare experiment with theory. This exploratory model allows to advance estimates for the onset of vanishing excitonic states for a given crystallite size and composition. Furthermore, it is possible to estimate the effect of different host materials—where the crystallites are embedded—on the exciton behavior. Indeed, as is the case with any exploratory model, one must be aware of its limitations. Aspects such as a size-dependent dielectric function, charge polarization at the crystallite surface, non-parabolicity of the energy band, etc. were not taken into account here. However, the general agreement observed for the gross behavior of the excitonic ground state energy as a function crystallite size seems far from being fortuitous.

4. Properties of dense molecular hydrogen

As a third example of the use of exploratory models in the analysis of problems in condensed-matter physics, let us briefly discuss the case of matter under high pressures. In particular, we shall be concerned with the case of molecular hydrogen, whose properties at high pressures are still subject of intense study and controversy [43].

Studying the properties of the simplest neutral molecule (H_2) under high pressures may serve as a starting point to understand the corresponding behavior of more complicated molecules. Several theoretical and experimental groups have devoted important efforts to the study of pressure-induced phase transitions in solid and liquid hydrogen [44–50]. A complete phase-diagram for hydrogen is still under construction [51]. Still some controversy on the onset of metallization to require of an intermediate atomic state or directly taking place from the molecular state, is going on [44–46, 52, 53]. Hence, in spite of being the simplest molecular system, understanding solid/liquid H_2 under high pressures has become a challenging issue in condensed matter physics. Of course, a detailed analysis of this many-body problem requires of sophisticated treatments, such as quantum Monte Carlo methods [1], Ab initio molecular dynamics [2] and density functional theory [54, 55], to mention a few. However, still in this case, some simplifying assumptions may lead to tractable models with predicting capability. In the following we shall illustrate the use of a molecular confinement model [56] to investigate pressure effects on the ground-state energy, polarizability and vibrational properties of the hydrogen molecule.

4.1. The molecular confinement model

Consider a condensed medium (e.g. a dense liquid) where the intermolecular distances are small enough so that the surrounding molecules create a potential barrier for the electrons associated to a particular molecule embedded in the medium.

Thus an exploratory model for this system may consist in viewing a constituent molecule of the medium as a caged-in system within a given boundary with finite potential barrier height. The volume of the confining box is then associated to the density of the medium whose changes are in turn related to pressure. The height of the potential barrier defines the confining capacity of the medium and corresponds physicaly to the mean field where a particular molecule is embedded.

Just as in the case of excitonic behavior in quantum dots discussed in the previous section, here we have another interesting use of the concept of confined quantum systems. The reader is kindly addressed to an excellent review paper on this type of models by Jaskolski [57]. We note at this stage that the case of the hydrogen molecule confined within penetrable boundaries had not been treated before even using an exploratory model until recently [56]. In the foregoing a brief description of the model is given. In contrast with the previous sections, here we shall present some new results not published before.

Using the FSGO scheme—as described in Sect. 2—the H_2 molecule in its ground state is a two-electron system represented by a single Gaussian orbital centered at the origin [$\mathbf{R}_k = 0$ in Eq. (5)]. Now, consider the molecule confined by a penetrable spherical cage of radius R_c and potential barrier height V_0 at the boundary as depicted in Fig. 9 and assume the confining potential has the form:

$$V(r) = \begin{cases} 0 & (r \leq R_c) \\ V_o & (r > R_c). \end{cases} \tag{14}$$

Inclusion of the function $V(r)$ in the molecular Hamiltonian demands different expressions for the interior and exterior representation of a localized orbital so that the boundary matching conditions are satisfied. Hence the following representations for the interior and exterior FSGO are proposed:

$$\Phi_i(r) = N_i(e^{-ar^2} - e^{-bR_c^2}), \quad (r \leq R_c) \tag{15a}$$

$$\Phi_o = N_0 e^{-gr^2}, \quad (r > R_c) \tag{15b}$$

where a, b and g are orbital parameters to be determined after minimization of the total energy functional given by Eq. (8). The normalization factors and orbital parameters are related through the boundary and normalization conditions as:

$$N^0 = N^i[e^{(g-a)R_c^2} - e^{(g-b)R_c^2}], \tag{16a}$$

$$g = \frac{a}{[1 - e^{(a-b)R_c^2}]}. \tag{16b}$$

Note that the one-electron integrals $(j|k)$ and the two-electron Coulomb and exchange terms $(kl|pq)$ in Eq. (6) must be evaluated taking into account the domain of integration for the interior and exterior wavefunctions. Here the one-electron operator [Eq. (7c)] becomes

$$w = -\frac{1}{2}\nabla^2 + \begin{bmatrix} -|\mathbf{r} - \mathbf{R}_A|^{-1} - |\mathbf{r} - \mathbf{R}_B|^{-1} & (r \leq R_c) \\ V_o & (r > R_c) \end{bmatrix}, \tag{17}$$
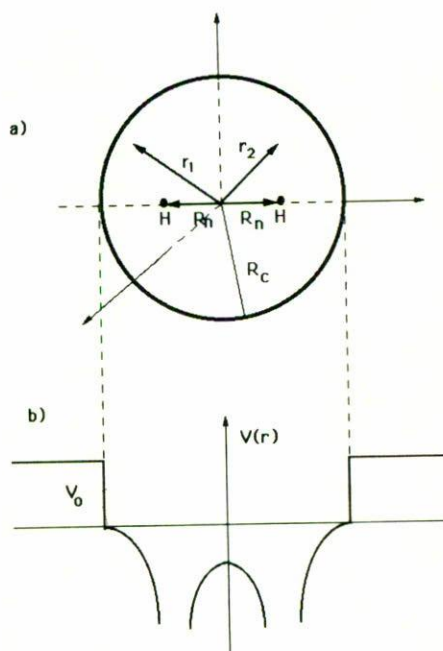
FIGURE 9. (a) H_2 molecule enclosed within a padded spherical box of radius R_c. The electron and nuclear positions are referenced to the center of the sphere. (b) Schematic representation of the confining potential barrier of height V_0.

where $\mathbf{r}$ and $(\mathbf{R}_A, \mathbf{R}_B)$ are the position vectors of an electron and a nucleus relative to the origin, respectively and $V(r)$ is given by Eq. (14).

In our case, since we only require of one orbital for each domain [Ecs. (15a) and (15b)], the total energy functional (W) may be easily evaluated analytically as a function of the orbital parameters (a, b, g), confining radius (R_c), nuclear position (R_n) and barrier height (V_0) [56]. The optimal values of the molecular parameters and the corresponding energy are found through a minimization procedure. Hence, given a certain barrier height, varying the confinement radius makes the energy values to change as well as the orbital radius and nuclear positions. In this sense, the calculation treats self-consistently both, electronic structure and molecular conformation as a function of confinement radius and barrier height.

4.2. Calculation of some molecular properties of dense molecular hydrogen

Considering molecular hydrogen in its liquid phase and taking the effective molecular volume as that of the confining sphere ($V_0 = 4\pi R_c^3/3$), the cold pressure ($T = 0K$) may be evaluated through changes in the total ground-state electronic energy as a function of confinement volume, i.e. $P = -\partial W/\partial V_0$, which in turn may be directly related to the density of the medium. Hence, some properties of molecular hydrogen as a function of pressure (density) and confining capacity of the medium (barrier height) may be surveyed.

TABLE V. Pressure dependence of the total energy, internuclear distance and average polarizability for the hydrogen molecule enclosed within an impenetrable spherical box obtained in this work. Values in parenthesis correspond to accurate calculations by Le Sar and Herschbach [58] for quasi-spherical boxes.

$2R_c$	Density	Pressure	Total Energy	Internuclear	Polarizability
(a_o)	(mol/cm^3)	(GPa)	$(hartrees)$	distance (a_o)	(a_0^3)
3.0	0.793	3700	0.7253	0.745	0.257
		(3500)	(0.6474)	(0.686)	(0.197)
4.0	0.333	690	-0.3331	0.944	0.695
		(770)	(-0.4749)	(0.893)	(0.509)
5.0	0.171	170	-0.7117	1.112	1.408
		(180)	(-0.8800)	(1.068)	(0.994)
6.0	0.099	48	-0.8613	1.248	2.328
		(55)	(-1.0441)	(1.208)	(1.606)
7.0	0.062	14	-0.9216	1.348	3.288
		(17)	(-1.1136)	(1.301)	(2.230)
8.0	0.042	3.9	-0.9448	1.414	4.083
		(5.9)	(-1.1440)	(1.355)	(2.769)
∞	0.036	0.0001	$-0.9559(4)$	1.474	4.924
			(-1.1716)	(1.403)	(4.196)

Le Sar and Herschbach (LH) [58] studied the properties of the hydrogen molecule enclosed within impenetrable ($V_0 = \infty$) prolate spheroidal boxes using a variational calculation with a five-term James-Coolidge wavefunction [59]. Interestingly, these authors found that the symmetry of the confining boxes for which the total energy is a minimum is practically spherical. Table V shows a comparison between the accurate calculations by LH and ours for total energy (W), internuclear distance ($D_e = 2R_n$) and average polarizability (α) as a function of pressure for this case. The values from LH are given within parenthesis. The average polarizabilities have been calculated using the method prescribed by LH, *i.e.* [58]:

$$\alpha = \frac{(\alpha_{\parallel} + 2\alpha_{\perp})}{3}, \tag{18}$$

where the parallel and perpendicular components are given as:

$$\alpha_{\parallel} = \alpha_{zz} = 8[\langle z^2 \rangle + \langle z_1 z_2 \rangle]^2, \tag{19a}$$

$$\alpha_{\perp} = \alpha_{xx} = \alpha_{yy} = 8[\langle x^2 \rangle + \langle x_1 x_2 \rangle]^2. \tag{19b}$$

In our case, a single spherical gaussian makes the anisotropic terms $\langle z_1 z_2 \rangle = \langle x_1 x_2 \rangle = 0$ and $\alpha_{\parallel} = \alpha_{\perp} = 8[\langle z^2 \rangle]^2$. The integrations implied by this expression are easily calculated taking into account the interior and exterior wavefunctions using Eqs. (15) and (16). Of course, quadrupole moments cannot be calculated with our approximate treatment.

Inspection of Table V indicates that our energy values are typically above by about 20% from those by LH, as expected

from the observations by Frost on the FSGO method (see Sect. 2). Whereas the internuclear distances and pressure values keep an overall fair agreement. Our calculated average polarizability as a function of box size shows a better agreement with those of LH for smaller box sizes. For intermediate values of R_c the difference observed with the corresponding LH values is due to the abscence of the anisotropic terms ($\langle z_1 z_2 \rangle$ and $\langle x_1 x_2 \rangle$) in our calculation. LH also calculated the location of potential minima for each box size and vibrational properties for the ground-state molecule after fitting the corresponding potential curves (V) around the minimum (r_e) using the Dunham expansion [58]:

$$V(x) = A_0 x^2 (1 + A_1 x + A_2 x^2) \tag{19}$$

with $x = (r - r_e)/r_e$. The Dunham parameters (A_0, A_1, A_2) are then used to calculate the rotational constant (B_e), vibrational frequency (ω_e), anharmonicity constant ($\omega_e x_e$) and Raman frequency ($\omega_R = \omega_e - 2\omega_e x_e$) with the following definitions [60, 61]:

$$B_e = \frac{h}{8\pi^2 \mu c D_e^2} = 119.539672 D_e^{-2} (cm^{-1}), \tag{21a}$$

$$\omega_e = \hbar^{-1}(4A_0 B_e hc)^{1/2}$$
$$= (4A_0 B_e)^{1/2}(468.481)(cm^{-1}), \tag{21b}$$

$$\omega_e x_e = \frac{\hbar^2}{48\mu D_e^2(hc)}[45A_1^2 - 36A_2],$$
$$= 4.998081965[45A_1^2 - 36A_2]D_e^{-2}(cm^{-1}), \tag{21c}$$

where D_e is the internuclear distance in atomic units, μ the reduced mass, h is Plancks constant ($\hbar = h/2\pi$) and c the speed of light in vacuum. A_0 is given in hartrees and A_1 and A_2 are dimensionless.

Table VI displays the box-size dependence of B_e, ω_e, $\omega_e x_e$, and ω_R as compared to those from LH (values within parenthesis) in the case of infinite barrier height. For completeness, the values for the Dunham parameters obtained here and the corresponding quantities from LH (parenthesis) are also presented. Except for the anharmonicity terms, a fair overall qualitative and quantitative agreement is observed for the rest of the quantities. Inspection of the Dunham parameters in Table VI shows larger differences between our A_2 values and those from LH. Since A_2 may be associated to deviations from a parabolic shape of the potential curve in the fitting region, the differences in the anharmonicity terms reflect this fact. Our potential energy curves are softer than the more accurate ones obtained by LH.

In spite of the simplicity of our exploratory model, the results analyzed so far are encouraging to assess reliable qualitative and quantitative information on the trend of the molecular properties of the system as a function of pressure (density). Of course, in the case of infinite barrier height, we have only compared the results of this model with a more sophisticated calculation to gain some confidence on its capabilities.

TABLE VI. Rotational constant (B_e), vibrational frequency (ω_e), anharmonicity constant ($\omega_e x_e$) and Raman frequency (ω_R) obtained in this work for the hydrogen molecule enclosed within impenetrable spherical boxes of different sizes. The associated Dunham parameters (A_0, A_1, A_2) are also included for completeness. Values in parenthesis are corresponding accurate calculations by Le Sar and Herschbach [58] for quasi-spherical boxes.

$2R_c$ (a$_o$)	A_0 (hartrees	A_1	A_2	B_e (cm^{-1})	ω_e (cm^{-1})	$\omega_e x_e$ (cm^{-1})	ω_R (cm^{-1})
3	1.54212	−1.02548	0.95805	215.38	17076	115	16845
	(1.7635)	(−0.7953)	(0.3456)	(253.71)	(19819)	(169)	(19481)
4	1.13881	−1.08069	1.03473	134.14	11581	86	11410
	(1.1594)	(−0.8080)	(0.3290)	(148.07)	(12276)	(108)	(12060)
5	0.89647	−1.13707	1.13267	96.67	8723	70	8582
	(0.9333)	(−0.9178)	(0.3213)	(104.68)	(9261)	(115)	(9031)
6	0.73685	−1.19326	1.22791	76.87	7052	64	6925
	(0.6221)	(−1.1345)	(0.6429)	(81.80)	(6684)	(118)	(6448)
7	0.62691	−1.24919	1.31654	65.78	6017	63	5892
	(0.5066)	(−1.2152)	(0.6888)	(70.59)	(5602)	(122)	(5358)
8	0.55099	−1.30662	1.42408	59.78	5378	64	5250
	(0.4431)	(−1.3759)	(0.9032)	(65.05)	(5030)	(142)	(4746)
∞	0.45809	−1.46408	1.90964	55	4703	64	4577
	(0.3661)	(−1.1653)	(1.7154)	(60.64)	(4415)	(138)	(4139)

TABLE VII. Properties of the hydrogen molecule confined within penetrable spherical boxes of different sizes and for selected barrier heights.

$2R_c$ (a$_o$)	Pressure (Gpa)	Total Energy (hartrees)	Internuclear distance (a$_o$)	Polarizability (a$_o^3$)	B_e (cm^{-1})	ω_e (cm^{-1})	$\omega_e x_e$ (cm^{-1})	ω_R (cm^{-1})
			V=0					
3.0	753	−0.6458	1.095	1.505	99.67	8725	98	8528
4.0	136	−0.8617	1.251	2.551	76.42	6964	73	6818
5.0	27	−0.9309	1.368	3.644	63.94	5847	62	5723
6.0	5	−0.9509	1.438	4.454	57.83	5162	60	5042
7.0	0.6	−0.9552	1.466	4.825	55.59	4828	72	4684
8.0	0.05	−0.9559	1.474	4.913	55.09	4727	85	4558
			V=0.25					
2.0	6537	0.2250	0.874	0.607	156.61	12444	165	12114
3.0	873	−0.5745	1.046	1.248	109.25	9542	97	9348
4.0	168	−0.8311	1.204	2.193	82.44	7555	72	7411
5.0	36	−0.9193	1.331	3.273	67.46	6261	58	6145
6.0	7	−0.9476	1.418	4.218	59.47	5410	52	5305
7.0	1	−0.9546	1.460	4.744	56.07	4923	60	4803
8.0	0.4	−0.9558	1.472	4.899	55.17	4747	79	4589
			V=1.0					
2.0	8328	0.6047	0.785	0.398	194.16	15207	158	14981
3.0	1149	−0.4240	0.962	0.898	129.10	11176	97	10982
4.0	234	−0.7682	1.128	1.687	94.01	8644	69	8506
5.0	55	−0.8949	1.270	2.713	74.17	7003	53	6898
6.0	13	−0.9398	1.379	3.766	62.87	5885	44	5798
7.0	2	−0.9530	1.445	4.548	57.25	5148	42	5065
8.0	0.2	−0.9556	1.469	4.859	55.38	4802	64	4673

Taking different barrier heights for the confining potential (V_0), the molecular properties discussed before may be surveyed within the exploratory model presented here. Table VII displays predicted values for pressure, total energy, internuclear distance, polarizability and vibrational constants for $V_0 = 0, 0.25$ and 1 a.u. Note that as the barrier height is reduced, the variation of all properties is less pronounced as the box radius is decreased. Figure 10 shows the predicted behav-
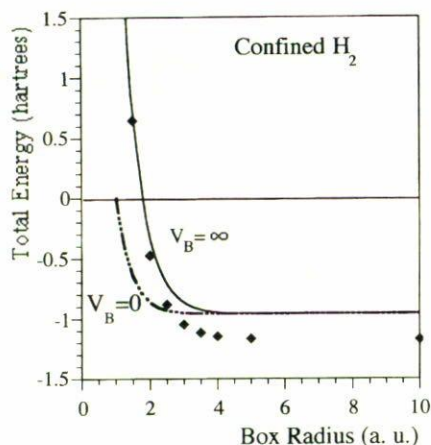
FIGURE 10. Total ground state energy of H_2 as a function of confinement radius for two extreme values of the confining potential. ($\blacklozenge$) "accurate" calculation [58] for $V_0 = 0$. Results of the work described here [56]: (—) $(V_0 = \infty)$, (- - -) $(V_0 = 0)$. (Replotted from Ref. 56).

FIGURE 11. Pressure-density curves for H_2 for two extreme values of the confining potential. ($\blacktriangle$) results from Ref. 58 for $V_0 = \infty$. Results of the work described here [56]: (- · - · -) $(V_0 = \infty)$, (—) $(V_0 = 0)$. (- - -) 0K isotherm for fluid H_2 [62]. (X) experimental EOS for solid H_2 at 80 K [50]. ($\Diamond$) temperature-reduced experimental EOS for solid H_2 [48]. Shock-compression experiments on fluid H_2: (O) [47], ($\triangle$) [53], ($\blacklozenge$) [52]. ($\square$) quantum monte carlo calculation for shock-compressed fluid H_2 [2].

ior of the total energy as a function of the confining radius for the two extreme barrier heights: $V_0 = \infty$ (continuous curve) and $V_0 = 0$ (chain curve). Also shown in this figure are the results by LH (solid diamonds) for the hard-wall case. From this figure we observe that for the lowest barrier height ($V_0 = 0$), the model predicts the appearance of a threshold box radius ($R_c \approx 1.025\, a_o$) below which no bound state for H_2 is available. This radius would correspond to a pressure of about 5200 GPa (see below), although this assertion is only speculative since it is quite possible that the system transits to a ionized and a further atomic state through previous excited-state channels.

An interesting feature of the exploratory model discussed here is its ability to render relevant physical information as the confining volume changes. In Fig. 11 the predicted pressure-density curves for molecular hydrogen confined within hard-walls ($V_0 = \infty$) (chain curve) and "transparent" walls ($V_0 = 0$) (continuous curve) are shown. Full triangles correspond to the results from LH for their hard-wall model. The dashed curve represents the equation of state (EOS) for fluid molecular hydrogen (0 K) developed by Kerley [62]. Also shown are experimentally derived EOS by Evans and Silvera [50] (crosses) and by Hemley *et al.* [48] (open diamonds) for static compression of solid molecular hydrogen. Recent experimental shock-compression measurements of liquid molecular hydrogen by Nellis *et al.* [47] (open circles), Weir *et al.* [52] (solid diamond) and Holmes *et al.* [53] (open triangles) are included in Fig. 11 for comparison. Also, the corresponding theoretical predictions by Lenosky *et al.* [2] using a quantum monte carlo approach are included in this figure. As the reader must be aware, a much more realistic description of the EOS is obtained when a padded-wall model is used as compared to the hard-wall model. It is important to stress here that, since the confinement model discussed

here considers only changes in the electronic energy, strictly speaking, our pressure-density relation can only be compared to the $T = 0$ K isotherm. Quite surprisingly, an almost complete agreement is observed with the shock-compresion experiments and quantum monte carlo studies, although some scepticism should be kept in addressing conclusions in this case since thermal pressure effects are not considered in this model.

5. Concluding remarks

The use of exploratory models to analyze some complicated problems may be a valuable means to gain insight on the properties of the system under study. In this work we have described three different problems where a simplified treatment has rendered important physical information. Of course, using exploratory models one could expect only a gross description of the quantitative and qualitative features of the system, as well as the role of associated relevant parameters. However, this information may be useful to set up a more detailed calculation.

A slightly more detailed discussion was devoted to the treatment of the properties of molecular hydrogen under high pressure, since new results are presented for this case. In this connection, the molecule-in-a box model with penetrable walls seems promising for the study of atomic and molecular systems under high pressures. A more formal, detailed calculation for this case demands by far a considerably larger effort and still is not available. This, together with the exciton confinement problem treated in Sect. 3, points to a useful characteristic of models based on quantum confinement.

1. D.M. Ceperley and B. Adler, *Science* **231** (1986) 555; D.M. Ceperley and B. Adler, *Phys. Rev. B* **36** (1987) 2092 and references therein.

2. T.J. Lenosky, J.D. Kress, L.A. Collins, and I. Kwon, *Phys. Rev. B* **55** (1997) 11907.

3. S.A. Cruz, *Radiat. Eff.* **88** (1986) 159.

4. H.A. Bethe, *Ann. Phys.* **5** (1930) 325; H.A. Bethe and R. Jackiw, *Intermediate Quantum Mechanics*, Third Edition, (Addison-Wesley, Massachusetts, 1997) Chap. 17.

5. H. Paul and M.J. Berger, in *Atomic and Molecular Data for Radiotherapy and Radiation Research* (International Atomic Energy Agency, IAEA-TECDOC-799, Vienna, 1995).

6. D.I. Thwaites, *Radiat. Res.* **95** (1983) 495.

7. D.I. Thwaites, *Nucl. Instrum. Methods Phys. Res. B* **12** (1985) 84; **27** (1987) 293; **69** (1992) 46.

8. P. Bauer, W. Rössler, and P. Mertens, *Nucl. Instrum. Methods Phys. Res. B* **69** (1992) 46.

9. P. Bauer *et al.*, *Nucl. Instrum. Methods Phys. Res. B* **136/138** (1998) 103.

10. R. Kreutz, W. Neuwirth, and W. Pietsch, *Phys. Rev. A* **22** (1980) 2598 and 2606.

11. J.F. Ziegler and J.M. Manoyan, *Nucl. Instrum. Methods Phys. Res. B* **35** (1988) 215.

12. J.R. Sabin and J. Oddershede, *Nucl. Instrum. Methods Phys. Res. B* **27** (1987) 280.

13. J. Oddershede and J.R. Sabin, *Nucl. Instrum. Methods Phys. Res. B* **42** (1989) 7.

14. S.A. Cruz and J. Soullard, *Nucl. Instrum. Methods Phys. Res. B* **61** (1991) 433; 71 (1992) 387.

15. J. Soullard, S.A. Cruz, and R. Cabrera-Trujillo, *Nucl. Instrum. Methods Phys. Res. B* **80/81** (1993) 20.

16. S.A. Cruz, J. Soullard, and R. Cabrera-Trujillo, *Nucl. Instrum. Methods Phys. Res. B* **83** (1993) 5.

17. D.N. Bernardo, *Phys. Rev. A* **39** (1989) 5532.

18. A.C. Diz, Y. Öhrn and J.R. Sabin, *Nucl. Instrum. Methods Phys. Res. B* **96** (1995) 633.

19. O.B. Firsov, *Zh. Eksp. Teor. Fiz.* **36** (1959) 1517; *Sov. Phys.-JETP* **9** (1959) 1076.

20. S.A. Cruz *et al.*, *Phys. Rev. A* **27** (1983) 2403.

21. J. Lindhard, *K. Dan. Vidensk. Selsk. Mat. -Fys. Medd.* **28** (1954) No. 8.

22. J. Lindhard and M. Scharff, *Phys. Rev.* **124** (1961) 128.

23. D.K. Brice and S.A. Cruz, *Radiat. Eff. Lett.* **43** (1979) 143.

24. A.A. Frost, *Theor. Chim. Acta* **18** (1970) 156 and references therein.

25. R. Mc Weeny, *Coulsons Valence*, Third Edition, (Oxford University Press, 1979) Chap. 13.

26. E. Clementi and C. Roetti, *At. Data Nucl. Data Tables* **14** (1974) 177.

27. S.Y. Chu and A.A. Frost, *J. Chem. Phys.* **54** (1971) 764.

28. J.L. Marin, R. Riera, and S.A. Cruz, *J. Phys.: Condens. Matter* **10** (1998) 1349.

29. Y. Wang and N. Herron, *J. Phys. Chem.* **95** (1991) and references therein.

30. Y. Wang and N. Herron, *Phys. Rev. B* **42** (1990) 7253.

31. G.T. Einevoll, *Phys. Rev. B* **45** (1992) 3410 and references therein.

32. Y. Kayanuma and H. Momiji, *Phys. Rev. B* **41** (1990) 10261.

33. Y. Kayanuma and K. Kuroda, *Appl. Phys. A* **53** (1991) 475.

34. P.E. Lippens and M. Lanoo, *Phys. Rev. B* **41** (1990) 6079; **39** (1989) 10935.

35. S.K. Nair, S. Sinha, and K.C. Rustagi, *Phys. Rev. B* **35** (1987) 4098.

36. L.E. Brus, *J. Chem. Phys.* **79** (1983) 5566.

37. H.M. Schmidt and H. Weller, *Chem. Phys. Lett.* **129** (1986) 615.

38. J.L. Marin and S.A. Cruz, *J. Phys. B: At. Mol. Opt. Phys.* **24** (1991) 2899.

39. J.L. Marin and S.A.Cruz, *J. Phys. B: At. Mol. Opt. Phys.* **25** (1992) 4365.

40. W.L. Wang and A. Zunger, *Phys. Rev. B* **53** (1996) 9579.

41. Y. Wang, A. Suna, W. Mahler, and R. Kasowski, *J. Chem. Phys.* **87** (1987) 7315.

42. A.I. Ekimov, Al.L. Efros, and A.A. Onuschehenko, *Solid State Commun.* **56** (1985) 921.

43. H.K. Mao and R.J. Hemley, *Rev. Mod. Phys.* **66** (1994) 671.

44. E. Kaxiras, J. Broughton, and R.J. Hemley, *Phys. Rev. Lett.* **67** (1991) 1138.

45. W.R. Magro, D.M. Ceperley, C. Pierleoni, and B. Bernu, *Phys. Rev. Lett.* **76** (1996) 1240.

46. M. Ross, *Phys. Rev. B* **54** (1996) 9589.

47. W.J. Nellis, S.T. Weir, and A.C. Mitchell, *Phys. Rev. B* **59** (1999) 3434.

48. R.J. Hemley *et al.*, *Phys. Rev. B* **42** (1990) 6458.

49. P. Loubeyre *et al.*, *Nature (London)* **383** (1996) 702.

50. W.J. Evans and I. Silvera, *Phys. Rev. B* **57** (1998) 14105.

51. W.B. Holzapfel, *Rep. Prog. Phys.* **59** (1996) 29.

52. S.T. Weir, A.C. Mitchell, and W.J. Nellis, *Phys. Rev. Lett.* **76** (1996) 1860.

53. N.C. Holmes, M. Ross, and W.J. Nellis, *Phys. Rev. B* **52** (1995) 15835.

54. S. Chakravarty, J.H. Rose, D. Wood, and N.W. Ashcroft, *Phys. Rev. B* **24** (1981) 1624.

55. N.W. Ashcroft, *Phys. Rev. B* **41** (1990) 10963.

56. S.A. Cruz, J. Soullard, and E.G. Gamaly, *Phys. Rev. A* **60** (1999) 2207.

57. W. Jaskolski, *Physics Reports* **271** (1996) 1.

58. R. Le Sar and D.R. Herschbach, *J. Phys. Chem.* **85** (1981) 2798; **87** (1983) 520.

59. H.M. James and A.S. Coolidge, *J. Chem. Phys.* **1** (1933) 825.

60. G. Herzberg, *Molecular Spectra and Molecular Structure: Spectra of Diatomic Molecules*, second edition, (Krieger Publishing Co., New York, 1989).

61. C.H. Townes and A.L. Schawlow, *Microwave Spectroscopy*, (Mc Graw-Hill, New York, 1955).

62. G.I. Kerley, in *Molecular-Based Study of Fluids*, edited by J.M. Haile and G.A. Mansoori, (American Chemical Society, Washington, D.C., 1983) p. 107.